Aerosols under heatwaves: Interactions between pollution and heatwave extremes

[1]Caushaj, Megi, [2]Mandija, Floran, [2]Keckhut Philippe, [2]Alraddawi Dunya, [1]Premti, Dhurata; [3]Miço, Silvana; [4]Frasheri, Neki; [4]Vila, Floran
[1]Department of Chemistry, University of Tirana, 1001, Tirana, Albania
[2]Laboratoire Atmosphères, Observations Spatiales (LATMOS), Institut Pierre-Simon Laplace (IPSL), Université de Versailles-Saint-Quentin-en-Yvelines (UVSQ)/Paris-Saclay University, Sorbonne University, Centre National de la Recherche Scientifique (CNRS), 78280 Guyancourt, France
[3]Department of Physics, University of Tirana, 1001, Tirana, Albania
[4]Academy of Sciences of Albania, Tirana, 1001, Tirana, Albania

Abstract. Air pollution frequently occurs in urban areas, often associated with heatwaves, especially during the warmer seasons, which produce an added risk to public health. We have analysed multi-decadal aerosol and meteorological data over the Tirana metropolitan region (1980–2024) to quantify how aerosol load in terms of aerosol optical thickness (AOT) responds during heatwave events. Using ERA5 reanalysis, MERRA-2 aerosol fields, and MODIS AOT products, we identify heatwaves with a daily T_{max} exceeding the 90th percentile (1981–2010 baseline), aggregate event metrics, and compute synoptic composites. Heatwaves are consistently associated with positive aerosol anomalies: mean AOT increases of ≈+0.10 and modelled $PM_{2.5}$ increases of 10–20 μg m^{-3} during event days. Multivariate analyses suggest that heatwave principal parameters explain a significant portion of the total aerosol variation ($r \approx 0.48$ for event peaks). Several coincidental occurrences of both extremes have been identified, and a special case is further analysed. These results highlight the importance of analysing heat and air quality extremes as coupled phenomena and using integrated warning and mitigation strategies in the areas at risk, such as urbanised and industrialised areas. .

1 Introduction

Atmospheric aerosols have been intensely investigated by several tools, from in-situ measurements up to remote sensing techniques [1-3]. Aerosols play a dual role in this context. On the one hand, atmospheric aerosols directly and indirectly impact the global radiative balance by scattering/absorbing solar radiation, and by modifying cloud properties, coverage and lifetime [4]. The anthropogenic aerosols are one of the most important components of air pollution known by the WHO and EPA, with fine particulate matter (PM2.5) causing premature mortality and morbidity among the population [5]. Thus, analyses of the high aerosol load under extreme high temperatures, such as heatwaves, are crucial for both climate and health studies.

© The Authors, published by EDP Sciences. This is an open access article distributed under the terms of the Creative Commons Attribution License 4.0 (https://creativecommons.org/licenses/by/4.0/).

Several studies have reported the elevated aerosol burden events under heatwave conditions over Mediterranean basin [6-9]. Heatwaves are not only characterised by anomalous high temperatures, but these phenomena are generally associated with persistent high-pressure and atmospheric blocking systems. Blocking systems reduce air ventilation and vertical mixing, which leads to higher accumulation of pollutants near the surface [10, 11]. Lower planetary boundary layer heights during heatwaves further intensify near-surface pollutant concentrations. At the same time, under higher temperatures and increased solar radiation, especially during the summer season, photochemical processes are favoured, enhancing the formation of secondary aerosols [12, 13]. The combination of the two events establishes positive feedback between heatwaves and aerosol burden.
The Mediterranean region's high anthropogenic emission concentrations, summer isolation, and climatological blocking make it especially vulnerable to these compound extremes [14-16]. Previous case studies have reported events where intense heatwaves coincided with major aerosol burden [18, 19]. However, systematic multi-decadal assessments of heatwave–aerosol interactions remain limited, especially in the Mediterranean region, where observational networks are sparser and integrated datasets are only recently becoming available.

This study focuses on Tirana, a fast-expanding Mediterranean-continental urban area, and examines; how aerosol loads behave during heatwaves, what synoptic conditions favour their co-occurrence, and the role of the urban environment in modulating these interactions. We aim to address this gap by providing a comprehensive analysis of aerosol vs. heatwave interactions over the Tirana region, combining multi-decadal satellite aerosol optical thickness (AOT) products and reanalysis meteorological fields. Specifically, we construct a catalogue of heatwave events based on the 90^{th} percentile exceedance criterion relative to the 1981–2010 baseline and quantify composite anomalies of AOT and temperature. By integrating multiple datasets and statistical approaches, we provide new insights into the processes that link extreme heat to pollution peaks in this southern European region.

The main results of this work contribute to deepening the overall knowledge on ensemble climate–air pollution extremes. These findings are relevant to both the atmospheric research community and the policymakers engaged in the management of climate adaptation and public health. With heatwaves projected to be even more frequent and severe under global warming scenarios [20], understanding the behaviour of aerosols under the extreme conditions is important for developing effective warning systems and mitigation strategies.

2 Data and Methods

This section describes the domain, timespan, datasets, heatwave event detection procedure, and analytical and statistical methods used to investigate the variation of the heatwave and aerosol burden extremes and their correlation.

2.1 Study period and spatial domain

The analysis focuses on the Tirana metropolitan area and a surrounding regional domain large enough to capture the characteristics of aerosol loads and synoptic patterns (41.1°N–41.5°N, 19.80°E–20.1°E). The region under investigation is the city of Tirana, capital of Albania, its surrounding suburbs. To make necessary comparisons, the surrounding rural areas have been taken into account in these analyses. The study period spans 1980–2024; in most analyses, we use the full reanalysis dataset for the entire period and extend to the latest available ERA5 data where applicable.

2.2 Meteorological and Aerosol Data

We use ERA5 (ECMWF) reanalysis [21] for meteorological diagnostics, including: 2m, 10m, and tropopause temperatures (monthly), wind speed (for ventilation and stagnation metrics), planetary boundary layer (PBL), mean sea-level pressure (MSLP), and 500-hPa geopotential height for synoptic composites and blocking diagnostics. Maximal values of 2 m temperature T_{max} are used for heatwave detection.

ERA5 fields were downloaded on the native 0.25-degree grid and aggregated to daily means or maxima as required. For composite maps, ERA5 variables are re-gridded to a common 0.25-degree grid and spatially cropped to the regional domain.

For surface exposure and chemical interpretation, we used the outputs of the regional MERRA model, version 2 [22]. We primarily use columnar aerosol optical thickness (AOT at 550 nm) as a proxy for aerosol loading. Additionally, we have also analysed Angstrom exponent (AE at 440-870 nm) of aerosols to identify their size, and consequently their type and origin.

Satellite sources include MODIS (Terra/Aqua) Level-2/Level-3 AOT products (MOD04/MYD04), for long-term time series and spatial composites; use the Collection 6+ products unless otherwise specified. Meanwhile, Giovanni products [23, 24] were used to extract and visualise regional AOT and temperature fields, and the heatwave's parameters.

2.3 Statistical Methods

Heatwaves were detected from the gridded T_{max} time series using the following the percentile-based heat wave index [25]:

- Compute the 90^{th} percentile threshold for each calendar day from the 1981–2010 period.
- Identify days where T_{max} exceeds the threshold.
- Group consecutive days into events; a valid heatwave requires at least three consecutive exceedance days.

For each event, compute event-level metrics: start and end dates, duration, mean T_{max} anomaly, maximum daily T_{max} during the event, and mean event-aggregated AOT and PM values. Here, we retained ERA5 fields and computed statistics over event days. Blocking indices (Tibaldi-Molteni) were used to quantify blocking persistence during heat events [26].

Table 1. Heatwave principal parameters by definition: frequency, duration, and intensity.

Type	Short name	Definition	Units
Frequency	HWF	Frequency of heatwave events	Event
Duration	HWD	Maximum duration of heatwave events	Day
Severity/Intensity	HI	Max. temperature during heatwave events	°C

Three principal parameters of heatwaves have been analysed in this paper: heatwave frequency, duration and intensity (Table 1). These parameters have also been coordinated with the aerosol properties. To assess their correlations and mutual impacts.

2.4 Statistical Methods

We employed linear regression and Pearson correlation analysis to quantify the relationships between temperature metrics (e.g., surface air temperature, heatwave amplitude), heatwave events (HWF, HWD, HWI) and aerosol burden (in terms of AOT). Statistical significance was assessed at the $p < 0.001$ level.

In addition, principal component analysis (PCA) is performed to identify the principal factors (PCs) that represent the original variables and reduce the analysis dimensions [27, 28]. Determination of principal components was based on Kaiser's criterion.

Further on, the obtained PCs are used as input for the K-means clustering technique [29]. The clustering procedure was done after evaluating the optimal number of clusters, using the statistic gap method [30]. Clustering ensembles the data within the groups with similar properties, and the properties among different clusters are the most distinct possible.

To determine the major coincidence extremes, we have scored the co-occurrence of HWI and AOT. HWI is given as the cumulative heatwave intensity, which is given as the product of temperature exceedance from 90th percentile with the number of days (Kelvin or °C × days).

For each month, standardized values of AOT, HWI, and combined are calculated:

$$z_{AOT} = \frac{(AOT - mean(\text{AOT,na.rm=TRUE}))}{st(AOT, na.rm=TRUE)} \quad (1)$$

$$z_{HWI} = \frac{(HWI - mean(\text{HWI,na.rm=TRUE}))}{st(HWI, na.rm=TRUE)} \quad (2)$$

$$z_{sum} = \frac{1}{N} z_{AOT} + z_{HWI} \quad (3)$$

The score (standardized anomaly) is unitless and is calculated as the mean of $_{sum}$, and measures the joint extremeness of AOT and HWI. Large positive scores during these extreme events, suggest that, on average, during these events, both AOT and HWI are well above their long-term mean.

3 Results and Discussions

3.1 Heatwave Catalogue and Characteristics

To determine heatwaves, we have used a 90th percentile exceedance criterion relative to the 1981–2010 baseline. This resulted in the identification of 45 heatwave events during this period. Heatwave durations ranged from 3 to 15 days, with a mean of 7 days and a standard deviation of about 2 days. The histogram of the number of consecutive days satisfying the heatwave criteria (Fig. 1) Shows that the majority of these events lasted for less than 6 days, while only a smaller fraction of these events exceeded 10 days. Nevertheless, this is not exactly a heatwave event duration, which require more than 3 consecutive days. Taking this fact into account, heatwave event durations ranged mainly in the interval of 3 up to 6 days.

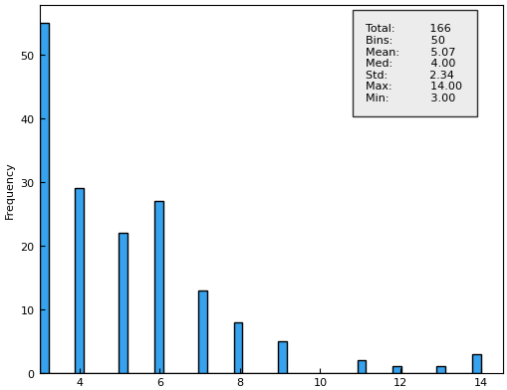

Fig. 1. Histogram of durations (days) of heatwave events (1980-2024) identified using the 90th percentile exceedance criterion. Here is presented the number of the largest number of consecutive days satisfying the heatwave criteria. Most events lasted 5-8 days, with a non-negligible portion of longer events (>10 days).

These findings are consistent with analyses over Europe reporting an increase in both frequency and intensity of heatwaves after the late 20th century [31, 32]. The frequency of medium-duration (5–8 days) events indicates that most episodes are driven by long-lasting synoptic-scale anomalies rather than transient weather changes. The significant increase in frequency and magnitude of the heatwaves (Fig. 2), especially after 2010, aligns with the global warming trends, indicating a rising probability of the occurrence of both extreme events in this region.

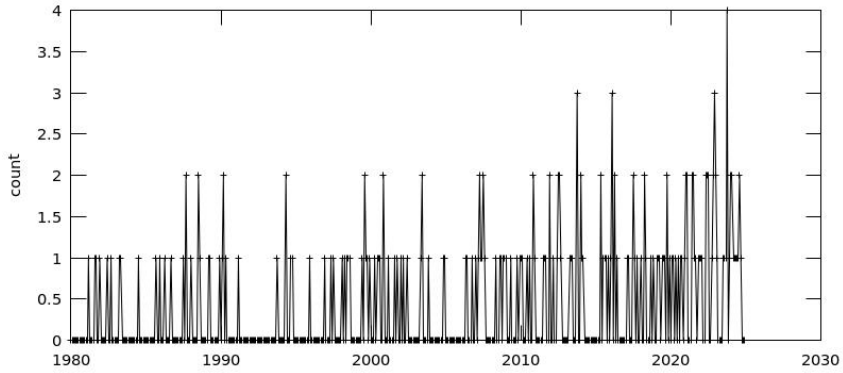

Fig. 2. Time series of the heatwave count of events satisfying the heatwave event criteria for the period (1980-2024).

The linear fitting equation of the heatwave counts over time is 0.008·x-0.23 (R^2=0.14). A very low value of the slope indicates a very slight increase in the mean count of heatwave events during this period.

3.2 Aerosol anomalies during heatwaves

In order to evidence the evolution and trends of the aerosol burden over Tirana during the period 1980-2024, we have used the time series of monthly mean Total Aerosol Optical Thickness (AOT_550), shown in Fig. 3. The overall decline after 1990 may be attributed more to effective regional emission control policies. This doesn't affect the positive feedback of these two extremes. The abrupt pollution peaks during heatwaves can be treated as episodic cases, also representing a tendency as well.

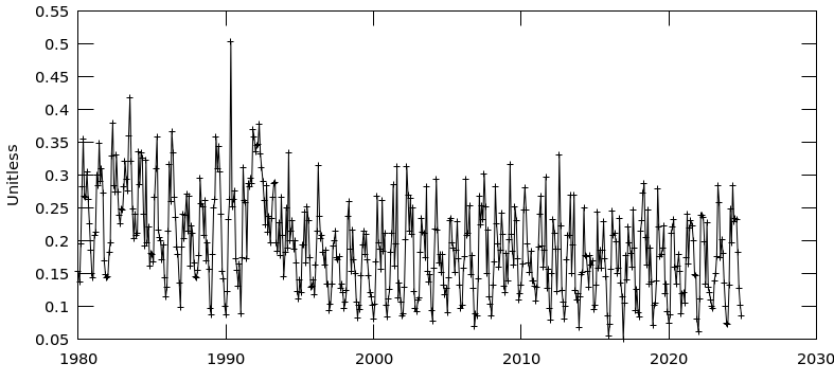

Fig. 3. Time series of monthly mean Total Aerosol Optical Thickness (AOT_550) over the Tirana region during the 1980-2024 period.

Composite analyses indicate consistent positive aerosol anomalies during heatwave days. Mean AOT over the Tirana urban area increased by approximately +0.10, while modelled surface PM2.5 concentrations increased by 10–20 μg m^{-3}, with some events approaching 40 μg m^{-3}.

Because of the long-term increase of the frequency of heatwaves and the decrease of the aerosol burden, a negative slope trendline characterized the scatterplot between these two paraments (Fig. 4). The slopes of the trendlines result to be different for the different aerosol optical depths. R^2 values are insignificantly small in all groups, so AOT explains very little of the variance in HWF in this dataset.

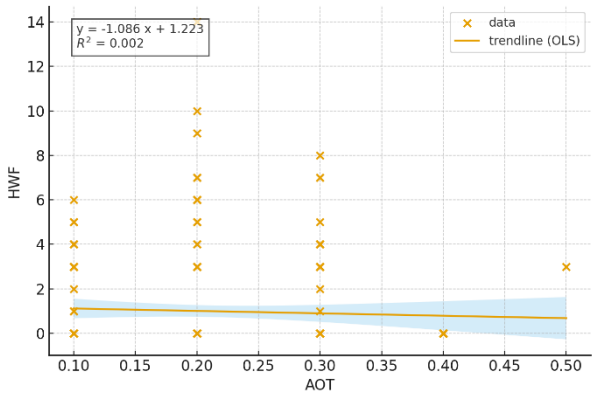

a)

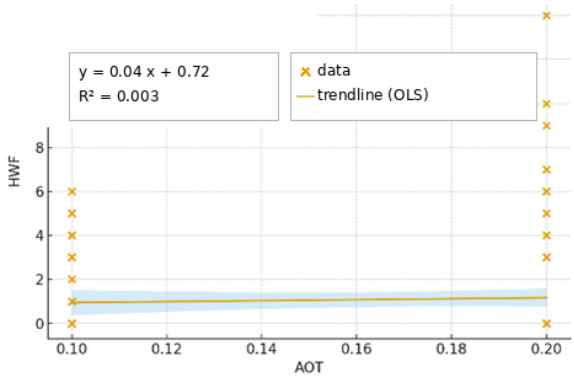

b)

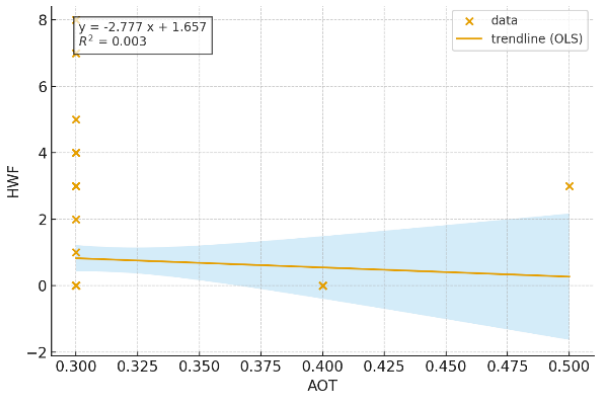

c)

Fig. 4. Long-term trends of heatwave frequency of occurrence (HWF) on aerosol optical depth (AOT_550). A) all AOT range., B) data of the 75th percentile of AOT among points with AOT > 0.01 and used that as the threshold. C) the remaining data of the dataset.

Such AOT anomalies are consistent with the dynamical and chemical processes known to govern heatwaves. Reduced ventilation and elevated isolation permit pollutants to accumulate, while associated with high temperature conditions, the secondary aerosol formation is accelerated. It is well known that elevated ozone levels during heatwaves stimulate the production of secondary organic aerosols. Thus, the relationship between heatwave parameters and aerosol burden is a cause-and-effect process, putting into play the physical and chemical mechanisms.

3.3 Synoptic drivers and boundary-layer processes

Composite meteorological fields reveal the dynamical origins of these anomalies. Heatwaves were characterised by anticyclonic conditions. Mean wind speeds at surface level during the heatwaves in this region were reduced by 1–2 m s^{-1}, while the planetary boundary layer height (PBL) decreased by 100–200 m. Both these reductions reflect atmospheric blocking, which reduces ventilation and confines pollutants to a thin PBL, augmenting the pollutant concentrations.

The time series of area-averaged number of the summer days (days per month when the daily maximum 2 m temperature exceeds 25°C) demonstrates a consistently high frequency of summer days throughout the dataset (Fig. 5). This provides a conducive background for heatwave formation and secondary aerosol production.

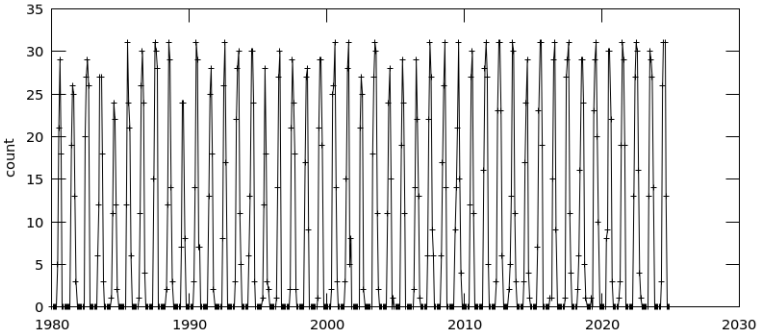

Fig. 5. Time series of the number of monthly summer days (3m temperature: T_{max} > 25°C). The persistently high number of summer days indicates a consistently warm summer climate in the region, which is normal for the eastern Mediterranean basin.

The evolution of monthly mean cloud top temperature is shown in Fig. 6. Over the last decades, the region has experienced a significant increase in surface temperature, consistent with global warming trends. Furthermore, the tropospheric temperature increases as well, resulting in warming of the entire tropopause layer. The small positive but significant slope is consistent with global warming, but the low R^2 indicates that internal variability and seasonal cycle are more dominant.

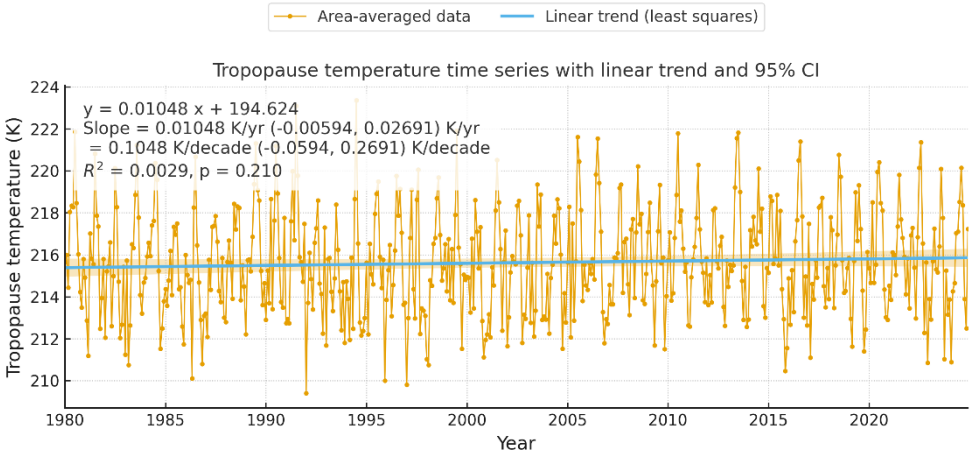

Fig. 6. Time series of area-averaged data monthly mean cloud top temperature (K), provided by MERA-2 reanalysis. Black points and orange line: monthly data; blue line: linear trend (1980–2024). Linear slope = +0.0105 K yr^{-1} (≈ +0.105 K $decade^{-1}$), R^2 = 0.0029.

Furthermore, our analysis indicates that during the coincidence cases of both extreme events, the urban heat island (UHI) effect in Tirana intensifies, with the urban area experiencing an average of 2.3 °C warmer temperatures than the surrounding rural areas (not shown graphically here). This urban heat island effect can further exacerbate heat stress and enhance photochemical reactions over the city of Tirana.

The importance of stagnation conditions in producing co-occurring extremes has also been previously reported. Our findings reinforce this, showing that blocking not only sustains high temperatures but also drives pollution accumulation. When it is combined with a shallow boundary layer, it amplifies even more the surface pollutant concentrations.

3.4 Regression analyses

Our analysis demonstrates significant positive relationships between aerosol optical thickness and surface air temperature and heat wave amplitude (Figs. 7 & 8). The scatter plot of monthly averaged surface air temperature against AOT reveals a statistically significant positive correlation ($R = 0.36$, $N = 540$, $p<0.001$).

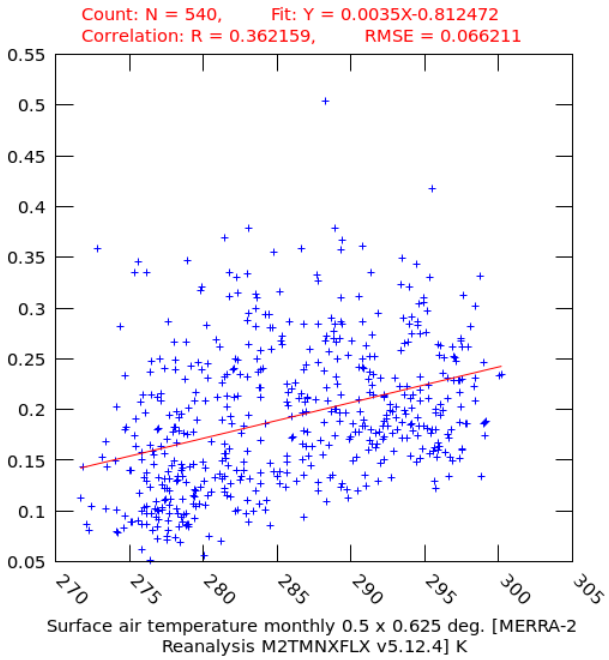

Fig. 7. Scatter plot of monthly averaged surface air temperature vs. Total aerosol extinction (AOT_550) during the 1980-2024 period. The significant high positive correlation ($R=0.36$, $p<0.001$, $N=540$) suggests a substantial tendency for aerosol accumulation under warmer conditions.

The strongest correlation between heatwave parameters and aerosol burden was found in the case of the heatwave intensity (HWI) and total aerosol extinction AOT_550 ($R = 0.48$, $N = 184$), as shown in Figure 8. This correlation indicates that the highest aerosol loads are encountered during significantly high temperatures. This significant correlation underscores that the intensity rather than just the occurrence of heatwaves is critical for aerosol enhancement. Weaker correlations were obtained between aerosol burden and other heatwave parameters (HWF and HWD). This fact suggests that the heatwaves parameters influence aerosol burden differently. The moderate correlation highlights the fact that even though the heatwaves increase the aerosol burdens, the variability in the aerosol emissions,

transport, and chemical regimes reduces the overall coefficient. This aligns with multi-city studies showing that the co-occurrence of both extreme events' probability is favoured but not deterministic [33-35].

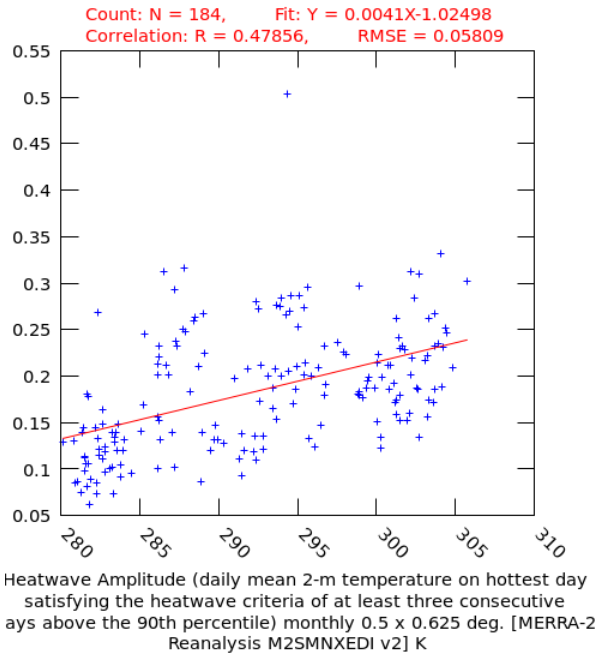

Fig. 8. Scatter plot of heatwave intensity (peak daily temperature during events) vs. Total aerosol extinction AOT_550 during the 1980-2024 period. The stronger correlation (R=0.48, p<0.001, N=184) supports even more that the intensity of a heatwave is a critical driver of the largest increases in aerosol pollution.

3.5 Major coincidence extremes (CE); case study

Table 2 presents the principal parameters of the twelve most important coincidence extremes. Among them, three major CEs have been identified during June and July 2007 and June 2021. We denominate these two coincident extremes as CE1 and CE.

Table 2. Top-12 major scores of commutative heatwave intensity (HWI) and mean aerosol optical depth (AOT). Start/end date, duration, mean AOT, temperature at 2 m, and Angstrom exponent for each event are presented.

No.	start_date	end_date	n_days	mean_AOT	mean_T2M	score
1.	8/17/2000	8/21/2000	5	0.63	26.8	2.25
2.	7/12/2001	7/14/2001	3	0.65	25.2	2.06
3	7/28/2001	7/30/2001	3	0.43	24.9	2.02
4	7/17/2003	7/19/2003	3	0.69	26.1	2.16
5	6/24/2007	6/26/2007	3	0.43	28.0	2.40
6	7/15/2007	7/20/2007	6	0.57	28.3	2.44
7	7/11/2011	7/13/2011	3	0.57	27.4	2.33
8	7/08/2012	7/20/2012	13	0.63	26.8	2.26
9	7/27/2012	7/29/2012	3	0.53	27.2	2.30
10	7/28/2020	7/30/2020	3	0.42	27.6	2.35
11	6/22/2021	6/24/2021	3	0.43	28.0	2.40
12	6/29/2021	7/1/2021	3	0.53	26.4	2.21

Particularly, we treat as a case study the situation of the period June-July 2007, when two major coincident extremes have occurred, having possibly different origins and properties. Both these two coincident extremes have the highest score.

Fig. 9 shows clearly that CE1 (24-26 June 2007) is characterized by significantly higher dust column mass density of almost 10 times. Meanwhile, CE2 (15-20 July 2007) is affected largely by black carbon, more than 4 times than CE1. CE2 has even more SO4 than CE, almost two times higher concentration. Table 3 shows average values of dust, black carbon and sulphate in these two intervals.

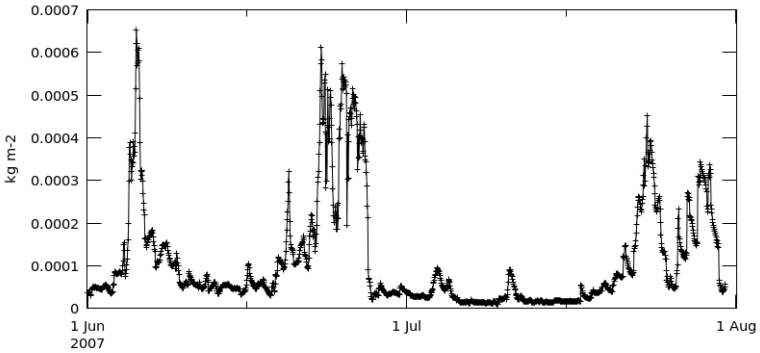

a)

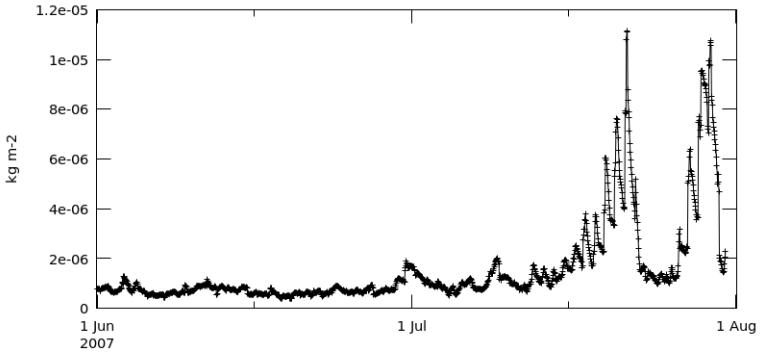

b)

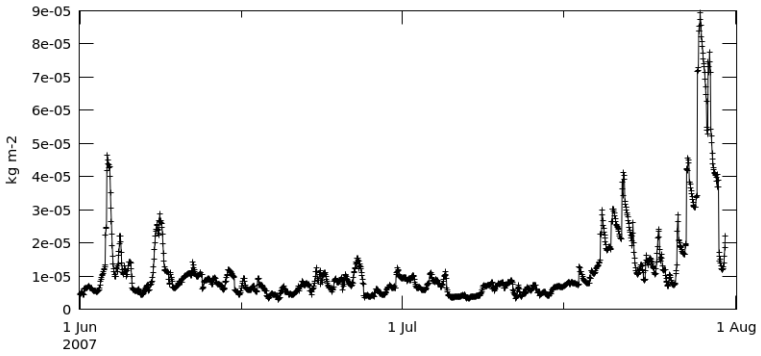

b)

Fig. 9. Time Series, Area-Averaged of a) Dust Column Mass Density, b) Black Carbon Column Mass Density, and c) SO4 Column Mass Density, time average hourly 0.5 x 0.625 deg. [MERRA-2 Reanalysis M2T1NXAER v5.12.4] kg m-2 over 2007-06-01 00Z - 2007-07-30 23Z, Region 19.7671E, 41.1312N, 20.1956E, 41.5267N.

Table 3. Area-averaged Column Mass Densities of dust, black carbon (BC), and sulphates (SO4), during the two coincidence extremes CE1 (24-26 June 2007) and CE2 (15-20 July 2007).

	Dust	**BC**	**SO4**	**AE**
CE1 (24-26 June 2007)	4.0·10-4	6.9·10-7	7.6·10-6	0.33
CE2 (15-20 July 2007)	3.4·10-5	2.9·10-6	1.3·10-5	1.63

Additionally, another important aerosol parameter, such as Angstrom exponent (AE_40-870 nm), show a much higher mean value during CE2 compared to CE1 (5 times higher), indicating the domination of the fine-mode aerosol particles during CE2, instead of coarse-mode aerosols during CE1.

Back-trajectories at 3 km altitude and AOT maps (Fig. 10) indicate that air masses during the first coincidence extreme over Tirana, come mainly from the Saharan desert, bringing mainly dust, which is consistent with other studies.

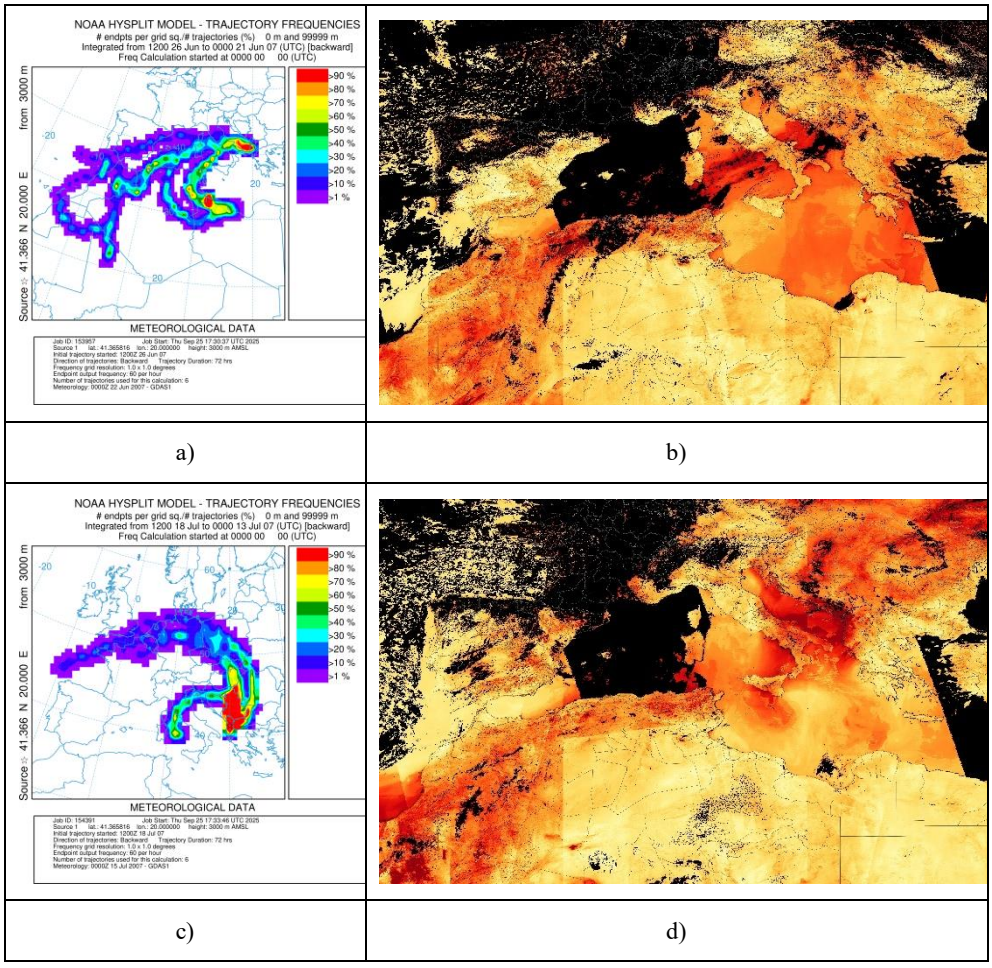

Fig. 10. NOAA Hysplit model – Trajectory Frequencies, 72 hr back-trajectories, Trajectory frequency grid resolution 1.0 deg. Level 1 height: 3000 m AMSL. Daily global distribution of Aerosol Optical Thickness (AOT) for b) 25 June 2007, d) 19 July 2007, obtained from NASA Worldview (https://worldview.earthdata.nasa.gov), using the MODIS-Aqua instrument data provided by NASA's Earth Science Data and Information System (ESDIS).

Meanwhile, air masses during the second coincidence extreme come from the central European region, bringing with them fine-mode aerosol originating from biomass burning over these regions. Even during SE2, dust originating from the north Africa region is still present over the western Balkans region.

Heatwave conditions favour uplift and long-range transport of dust and smoke. During the CE1 heatwave over Albania, persistent anticyclonic circulation enhanced surface heating, making the PBL more stable. Once mineral Saharan dust is transported over this region, it decreases atmospheric shortwave absorption and thereby contributes to the reduction of the persistence of heatwaves. Heatwave conditions during CE2, enhanced the natural fire activity, which together with agricultural biomass burning, yielded elevated emissions of black carbon from local and regional fires, which are favoured under stagnant synoptic regimes. Smoke aerosols are light-absorbing suppress convective mixing, which reinforces near-surface heating. However, the magnitude of absorption depends on aerosol optical properties, vertical profiles, and burden.

3.6 Multivariate Statistics

Among the principal parameters of heatwaves and aerosols, for a multivariate analyses, seven of them have been chosen; heatwave number, frequency and amplitude, surface and tropopause temperature, as well as aerosol optical depth and Angstrom exponent.

In the first step, the principal factor analysis (PCA), was performed over these seven variables. Three most important factors (PCs) cover all the seven variables, representing 80% of the total variance.

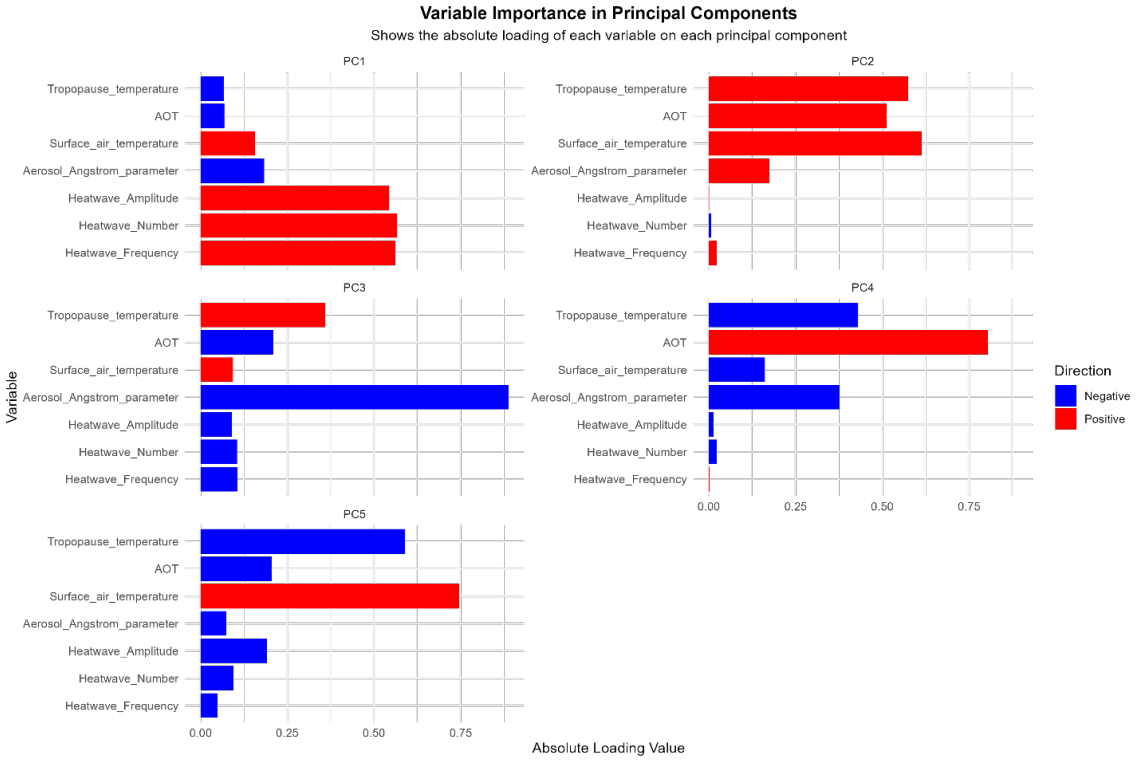

Fig. 11. Contributions of all, heatwave -, temperature- and aerosol variables into four principal factors (PCs). PC1 is contributed mainly by heatwave parameters, PC2 y temperatures, PC3 and PC4 by aerosol parameters (AOD_550) and (AE440-870).

PC1 loading from heatwave variables, and PC2 loadings from temperature variables and AOT, exceed value 0.50. Meanwhile PC3 loading from Angstrom exponent is very high, about -0.89. This situation is represented by Fig. 11. The Kaiser criterion suggests 2-3 principal components to be selected. So that PCs to represent all variables, three PCs have been chosen.

The Gap Statistics method to determine the optimal number of clusters, suggested to group the data of all variables into three clusters (Fig. 12).

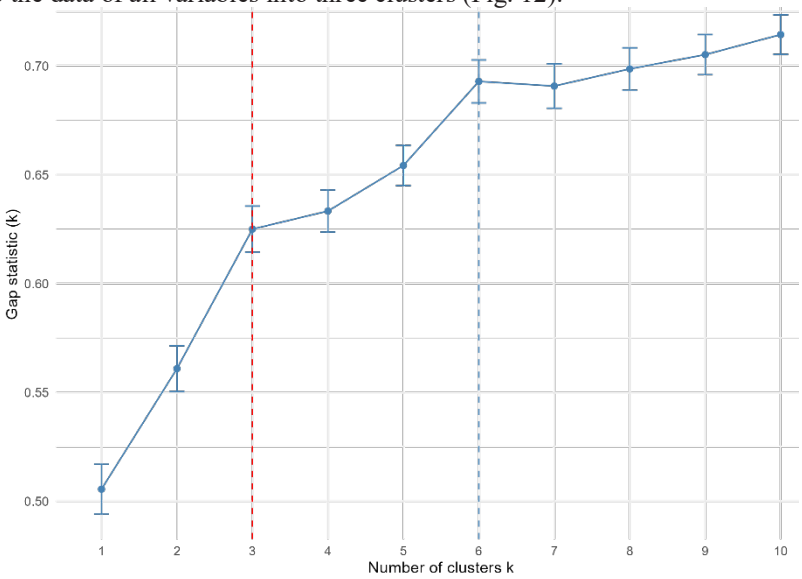

Fig. 12. Method of Gap-Statistics for determining the optimal number of clusters. Three main clusters have been suggested by this method.

Three clusters regrouping all data are presented in the form of convex hulls and density contours are presented in Fig. 13.

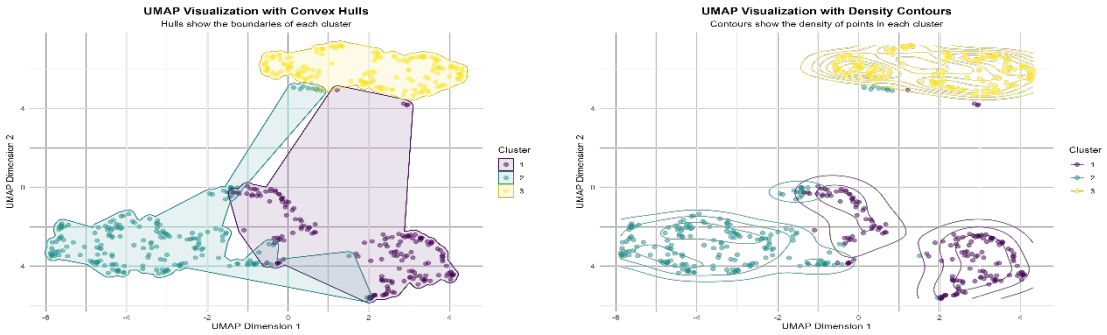

Fig. 13. Three main clusters identified by Gap Statistics method, using PCs instead of the using of original variables. Each of the three clusters contains 173 (I), 200 (II) and 167 (III) data respectively.

From the PCA results a closer correlation between heatwaves and also between temperatures (surface and tropopause) and AOT, have been indicated. However, a correlation matrix of the correlation coefficients (CC) should provide more details. Correlation coefficients have been retrieved based on their monthly-mean values. Fig. 14 presents a

correlation coefficient matrix among the original variables (Fig. 14.a) and also among the variables and the principal components (Fig. 14.b).

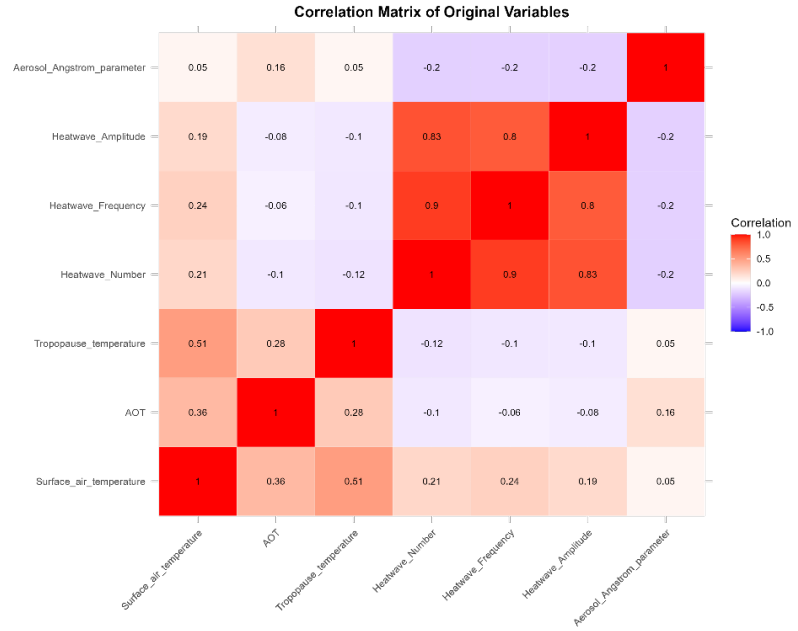

a)

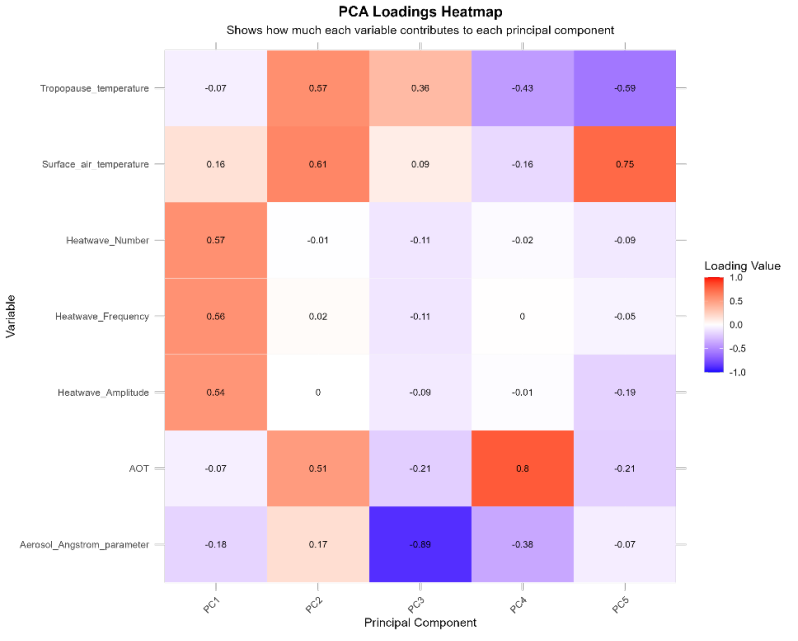

b)

Fig. 14. Correlation matrixes a) among the original variables and b) among the original variables and principal factors.

Heatwave parameters, such as frequency, number and intensity, exert strong positive correlations (CC: 0.80 ÷0.90), indicating that even one of these parameters, maybe sufficient to identify the heatwave presence. In addition, surface and tropopause temperatures result to be very correlated (CC: 0.51). This fact suggests that only one of these parameters is sufficient to be used for temperature characterizations of the heatwave conditions. Meanwhile, Angstrom exponent, which identifies aerosol size, results non significantly correlated with the other parameters.

The same picture is obtained also by correlation coefficients among variables and principal factors (Fig. 14.b). The heatwave parameters result in being strongly correlated with PC1. However, both temperatures, altogether with the AOT result to be correlated with PC2. This fact suggests that temperatures and AOT are represented by the same PC2, even though not being correlated with each other. To distinct AOT from temperatures, as variables with different physical properties, PC4 will serve as excellent representative for AOT, having a correlation coefficient of 0.80, much higher than that of PC2. In this case, we would have four PCs: PC1 representing only heatwave parameters, PC2 representing both temperatures, PC3 representing aerosol size (type), and PC4 representing aerosol burden.

Our findings align well with many recent studies in similar sites. The positive correlations between aerosol burden and heatwave parameters were found also in other regions affected by similar extremes [36]. The coupling of these extremes was observed over Poland, where AOT increased under atmospheric stagnation conditions and blocking anticyclones. Also, the variation of PBL observed in another study [37] affected AOT similarly to the case of this study. Furthermore, it was evidenced that positive radiative feedback of aerosols intensifies heatwave parameters [38], which is in synch with our results. Similar findings also have been obtained in other locations associated by different characteristics [39-43]. This consistency of the results across different regions defines the robustness of these findings.

3.7 Mechanistic synthesis and broader implications

Sensitivity analyses using nearby thresholds (such as 95th and 97.5th percentiles) show consistent results as in the case of the 90th threshold. This robustness across the thresholds indicates that the observed coupling is not forced by threshold choice.

Recent studies reported an increasing frequency of heatwaves in recent decades, consistent with global warming, especially over the Mediterranean region. This explains the observed consistent positive aerosol anomalies during heatwaves. The implications of these correlations are twofold. First, from a health perspective, combined exposures to heat and pollution affect health, especially for vulnerable groups (elders, children, people with chronic diseasesLow-income and socially disadvantaged populations, etc.), increasing risks of hospitalisations and premature mortality. Second, from a climate perspective, aerosols can modulate the radiative forcing under anormal high temperatures, providing positive feedback to the temperatures over the region.

The significant mutual interaction between these extremes, heatwaves and aerosol burden, underlines the necessity for integrated research on the forecasting models, to analyse them as coupled phenomena. They also stress the importance of mitigation: reducing urban emissions, lowering the UHI intensity through green introducing and expanding infrastructures, and improving monitoring networks.

A slight decline of AOT and an increase in the mean temperature were observed over a long-term period, suggesting a negative correlation between them. But, the positive correlation between them is attributed to short-term AOT anomalies under severe meteorological conditions.

4 Conclusions

This study provides a systematic multi-decadal climatology of heatwaves and aerosol burden over the Tirana city and surrounding areas. Furthermore, the analysis of the correlation between the parameters of these two extremes has been performed.
The combination of satellite-derived products on aerosol burden and ERA5 reanalysis meteorology have been employed to perform these tasks. Giovanni NASA platform was used to retrieve data on heatwave's parameters, aerosol optical thickness, and temperature in different pressure levels.
The analysis demonstrates these key findings:

- Aerosol burden enhancement during under high temperature conditions: We confirm that heatwaves over the Tirana region are generally associated with significant increase in aerosol load. Despite a long-term background decline in aerosols, and gradual increase of the mean temperature, aerosol extremes occur mainly during heatwaves. During these events the mean AOT increased by 0.10 and surface $PM_{2.5}$ concentrations by 10-20 $\mu g\ m^{-3}$.
- Synoptic and thermodynamic drivers: The co-occurrence of aerosol and temperature extremes is caused and associated by stagnant, anticyclonic conditions, that increased the accumulation of air pollutants, and consequently increase aerosol concentration.
- Representation: Principal component analyses and further clustering on PCs enabled to the reduce of the problem dimensionality and to visualize the principal data groups (clusters).
- Relationships: Correlations among the heatwave and aerosol variables and the representing principal factors have been determined, indicating the major inter-correlated variables.
- Intensity-driven correlation: Regression analysis confirmed a substantial positive relationship between peak temperature and aerosol optical depth, indicating that temperature amplitude has the strongest correlation particularly during the most intense heatwaves ($R = 0.48$). Thus, it revealed that the heatwave intensity, more than its occurrence, is crucial for increasing aerosol optical depth, and so, worsening the pollution conditions.

From the societal perspective, the co-occurrence of high temperatures and elevated air pollution (in terms of aerosol optical depth) rise the risks particularly for vulnerable groups of populations (above-mentioned cases). This makes indispensable the creation and development of integrated heat–air pollution warning and investigation systems. From the scientific perspective, this work highlights the importance of coupling multiple datasets to identify their interplay and their effects of the climate and population health.
Heatwave parameters, such as number, frequency and intensity, result to be closely correlated. The same pattern is observed for both surface and tropopause temperatures.
Future work should involve the investigation of even more aerosol and thermodynamic parameters, to better minimize the uncertainness about the interactions between these two extremes.

A special focus is set in the identification of coincidences between heatwaves and aerosol burden extremes. Top 12 major coincidence cases have been identified, and a special case is further analysed in detail, providing information about aerosol properties, their origins and pathways. This work aligns well with other studies that have reported positive feedback of anthropogenic aerosols on principal heatwave parameters. Recent policies, aligned with EU directives, foresee the development of national air quality plans, and investments in monitoring and public environmental health alerts.

It should taken into consideration, that although these analyses reveal a clear statistical correlation between heatwave parameters and aerosol burden, it does not establish a causal link between them. Identifying the physical processes that drive these relationships will require dedicated observational and modelling efforts to assess cause and effect.

In conclusion, as the frequency, duration and intensity of heatwaves are projected to increase due to climate change conditions, but the aerosol burden will be reduced due to the environmental policies, the uncertainties of the assessment of the compound risk posed by these two extremes could become important, making their joint investigation an emergent priority for both atmospheric science and environmental policy.

Data Availability Statement

The ERA5 reanalysis data are available from the Copernicus Climate Change Service (C3S) Climate Data Store (https://cds.climate.copernicus.eu/). The MERRA-2 data are available from the NASA Goddard Earth Sciences Data and Information Services Center (https://disc.gsfc.nasa.gov/). The MODIS data are available from the Level-1 and Atmosphere Archive & Distribution System (LAADS) Distributed Active Archive Center (DAAC) (https://ladsweb.modaps.eosdis.nasa.gov/).

References

[1] F. Mandija, P. Keckhut, D. Alraddawi, S. Khaykin, A. Sarkissian. Climatology of cirrus clouds over Observatory of Haute-Provence (France) using multivariate analyses on lidar profiles. Atmosphere **15**, 1261 (2024). https://doi.org/10.3390/atmos15101261

[2] F. Mandija, V. Chavez Perez, R. Nieto, M. Sicard, V. Danylevsky, J.-A. Anel Cabanelas, L. Gimeno. The climatology of dust events over the European continent using data of the Dust Regional Atmospheric Model. Atmos. Res. **209**, 144–162 (2018). https://doi.org/10.1016/j.atmosres.2018.03.006

[3] F. Mandija, K. M. Markowicz, O. Zawadzka. Characterization of aerosol events using synergistically column integrated optical aerosol properties and polarimetric measurements. J. Atmos. Solar-Terr. Phys. **150**, 9–20 (2016). https://doi.org/10.1016/j.jastp.2016.10.013

[4] O. Boucher, et al. Clouds and aerosols. In: Climate Change 2013: The Physical Science Basis. Contribution of Working Group I to the Fifth Assessment Report of the Intergovernmental Panel on Climate Change, pp. 571–657. Cambridge University Press (2013). A. J. Cohen, et al. Estimates and 25-year trends of the global burden of disease attributable to ambient air pollution. Lancet **389**, 1907–1918 (2017)

[5] J. Lelieveld, J. Evans, M. Fnais, et al. The contribution of outdoor air pollution sources to premature mortality on a global scale. Nature **525**, 367–371 (2015). https://doi.org/10.1038/nature15371

[6] F. Mandija, M. Caushaj, D. Premti, P. Keckhut, D. Alraddawi, N. Frasheri, F. Vila. Midlatitude spatial and temporal correlations between aerosol properties and weather extremes. Int. J. Environ. Pollut. (2025). https://doi.org/10.1504/IJEP.2025.10072437

[7] M. Chrit, K. Sartelet, J. Sciare, J. Pey, J. B. Nicolas, N. Marchand, E. Freney, K. Sellegri, M. Beekmann, F. Dulac. Aerosol sources in the western Mediterranean during summertime: a model-based approach. Atmos. Chem. Phys. **18**, 9631–9659 (2018). https://doi.org/10.5194/acp-18-9631-2018

[8] A. Pyrgou, P. Hadjinicolaou, M. Santamouris. Enhanced near-surface ozone under heatwave conditions in a Mediterranean island. Sci. Rep. **8**, 9191 (2018). https://doi.org/10.1038/s41598-018-27590-z

[9] G. K. Georgiou, T. Christoudias, Y. Proestos, J. Kushta, P. Hadjinicolaou, J. Lelieveld. Air quality modelling in the summer over the eastern Mediterranean using WRF-Chem: chemistry and aerosol mechanism intercomparison. Atmos. Chem. Phys. **18**, 1555–1571 (2018). https://doi.org/10.5194/acp-18-1555-2018

[10] S. Pfahl, H. Wernli. Quantifying the relevance of atmospheric blocking for co-located temperature extremes in the Northern Hemisphere on (sub-)daily time scales. Geophys. Res. Lett. **39**, L12805 (2012). https://doi.org/10.1029/2012GL052261

[11] P. M. Sousa, R. M. Trigo, P. Aizpurua, R. Nieto, L. Gimeno, R. Garcia-Herrera. Trends and extremes of drought indices throughout the 20th century in the Mediterranean. Nat. Hazards Earth Syst. Sci. 11, 33–51 (2011). https://doi.org/10.5194/nhess-11-33-2011

[12] M. Z. Jacobson. Atmospheric pollution: history, science, and regulation. Cambridge University Press (2002)

[13] A. M. Fiore, V. Naik, E. M. Leibensperger. Air quality and climate connections. J. Air & Waste Manag. Assoc. 65, 645–685 (2015).

[14] F. Mandija, M. Sicard, A. Comerón, L. Alados-Arboledas, J. L. Guerrero-Rascado, R. Barragán, J. A. Bravo-Aranda, M. J. Granados-Muñoz, H. Lyamani, C. M. Porcar, F. Rocadenbosch Burillo, A. Rodríguez, A. Valenzuela, D. G. Vizcaíno. Origin and pathways of the mineral dust transport to two Spanish EARLINET sites: effect on the observed columnar and range-resolved dust optical properties. Atmos. Res. **187**, 69–83 (2017). https://doi.org/10.1016/j.atmosres.2017.01.006

[15] D. Founda, M. Santamouris. Synergies between urban heat island and heat waves in Athens (Greece), during an extremely hot summer (2012). Sci. Rep. **7**, 10973 (2017). https://doi.org/10.1038/s41598-017-11407-6

[16] F. Mandija, F. Vila, E. Lukaj. Desert dust episodes over Balkan Peninsula. In: Proceedings of the 10th Balkan Physical Union. AIP Conf. Proc. **2075**, 130011 (2019). https://doi.org/10.1063/1.5091296

[17] A. Analitis, P. Michelozzi, D. D'Ippoliti, F. De'Donato, B. Menne, F. Matthies, R. W. Atkinson, C. Iñiguez, X. Basagaña, A. Schneider, C. Lefranc, A. Paldy, L. Bisanti, K. Katsouyanni. Effects of heat waves on mortality: effect modification and confounding by air pollutants. Epidemiology **25**, 15–22 (2014). doi.org/10.1097/EDE.0b013e31828ac01b

[18] F. S. Arsad, R. Hod, N. Ahmad, R. Ismail, N. Mohamed, N. Baharom, Y. Osman, M. F. M. Radi, F. Tangang. The impact of heatwaves on mortality and morbidity and the associated vulnerability factors: a systematic review. Int. J. Environ. Res. Public Health **19**, 16356 (2022). https://doi.org/10.3390/ijerph192316356

[19] IPCC. Climate Change 2021: The Physical Science Basis. Contribution of Working Group I to the Sixth Assessment Report. Cambridge University Press (2021)

[20] H. Hersbach, B. Bell, P. Berrisford, et al. The ERA5 global reanalysis. Q. J. R. Meteorol. Soc. **146**, 1999–2049 (2020). https://doi.org/10.1002/qj.3803

[21] R. Gelaro, W. McCarty, M. J. Suárez, et al. The Modern-Era Retrospective Analysis for Research and Applications, Version 2 (MERRA-2). J. Climate **30**, 5419–5454 (2017). https://doi.org/10.1175/JCLI-D-16-0758.1

[22] J. G. Acker, G. Leptoukh. Online analysis enhances use of NASA Earth science data. Eos Trans. AGU **88**, 14–17 (2007). https://doi.org/10.1029/2007EO020003

[23] R. C. Levy, S. Mattoo, L. A. Munchak, et al. The Collection 6 MODIS aerosol products over land and ocean. Atmos. Meas. Tech. **6**, 2989–3034 (2013). https://doi.org/10.5194/amt-6-2989-2013

[24] S. E. Perkins. A review on the scientific understanding of heatwaves—Their measurement, driving mechanisms, and changes at the global scale. Atmos. Res. **164–165**, 242–267 (2015)

[25] S. E. Perkins, L. V. Alexander. On the measurement of heat waves. J. Climate **26**, 4500–4517 (2013). https://doi.org/10.1175/JCLI-D-12-00383.1

[26] B. Dong, R. T. Sutton. Recent trends in summer atmospheric circulation in the North Atlantic/European region: is there a role for anthropogenic aerosols? J. Climate **34**, 6777–6795 (2021). https://doi.org/10.1175/JCLI-D-20-0665.1

[27] S. Lolli, P. Di Girolamo. Principal component analysis approach to evaluate instrument performances in developing a cost-effective reliable instrument network for atmospheric measurements. J. Atmos. Oceanic Technol. **32**, 1642–1649 (2015). https://doi.org/10.1175/JTECH-D-15-0085.1

[28] S. Liu, Y. Hu. Air quality prediction based on factor analysis combined with Transformer and CNN-BILSTM-ATTENTION models. Sci. Rep. **15**, 20014 (2025). https://doi.org/10.1038/s41598-025-03780-4

[29] M. J. McGrath, T. Olenius, I. K. Ortega, V. Loukonen, P. Paasonen, T. Kurtén, M. Kulmala, H. Vehkamäki. Atmospheric Cluster Dynamics Code: a flexible method for solution of the birth–death equations. Atmos. Chem. Phys. **12**, 2345–2355 (2012). https://doi.org/10.5194/acp-12-2345-2012

[30] B. Christiansen. Atmospheric circulation regimes: can cluster analysis provide the number? J. Climate **20**, 2229–2250 (2007). https://doi.org/10.1175/JCLI4107.1

[31] R. García-Herrera, J. Díaz, R. M. Trigo, J. Luterbacher, E. M. Fischer. A review of the European summer heat wave of 2003. Crit. Rev. Environ. Sci. Technol. **40**, 267–306 (2010). https://doi.org/10.1080/10643380802238137

[32] R. M. Trigo, D. Barriopedro, J. M. Garrido-Pérez, A. Simon, S. M. Plecha, A. Teles-Machado, A. Russo, R. Garcia-Herrera. The outstanding European and Mediterranean heatwave activity during summer 2022. Atmos. Res. **323**, 108195 (2025). https://doi.org/10.1016/j.atmosres.2025.108195

[33] C. Wang, X.M. Hu, S. Feron, J. Leffel, R.R. Cordero. Compound heat and ozone pollution in the urban environment. Urban Clim. **62**, 102511 (2025) doi.org/10.1016/j.uclim.2025.102511

[34] A. Piracha, M.T. Chaudhary. Urban air pollution, urban heat island and human health: a review of the literature. Sustainability **14**, 9234 (2022). doi.org/10.3390/su14159234

[35] P. Kumar, A. Chakraborty, A.K. Sagar. Impact of heatwaves on air pollutants in major climatic zones of India. Discov. Geosci. **3**, 119 (2025) doi.org/10.1007/s44288-025-00229-z

[36] I. S. Stachlewska, O. Zawadzka, R. Engelmann. Effect of heat wave conditions on aerosol optical properties derived from satellite and ground-based remote sensing over Poland. Remote Sens. **9**, 1199 (2017). https://doi.org/10.3390/rs9111199

[37] K. B. Betsy, S. K. Mehta. Role of aerosols on prolonged extreme heatwave event over India and its implication to atmospheric boundary layer. Atmos. Pollut. Res. **16**, 102513 (2025). https://doi.org/10.1016/j.apr.2025.102513

[38] A. Zhao, M. A. Bollasina, D. S. Stevenson. Strong influence of aerosol reductions on future heatwaves. Geophys. Res. Lett. **46**, 4913–4923 (2019). https://doi.org/10.1029/2019GL082269.

[39] C. Wang, Z. Li, Y. Chen, Y. Li, L. Ouyang, J. Zhu, F. Sun, S. Song, H. Li. Changes in global heatwave risk and its drivers over one century. Nat. Commun. **14**, 7691 (2023). https://doi.org/10.1038/s41467-023-43402-5.

[40] F. Chitsaz, A. Gohari, M.R. Najafi, M.J. Zareian, A. Torabi Haghighi. Heatwave duration and heating rate in a non-stationary climate: Spatiotemporal pattern and key drivers. Earth's Future **12**, e2023EF003995 (2023). https://doi.org/10.1029/2023EF003995.

[41] H. Ji, A. Feng, Y. Zhao, J. Liao, Z. Zhang, C. Gu, A. Feng. Characteristics of heat waves in mainland China since 1961 based on absolute and relative methods. Atmosphere **14**, 544 (2023). https://doi.org/10.3390/atmos14030544.

[42] S.-H. Lo, C.-T. Chen, H.-H. Hsu, M.-F. Shih, H.-C. Liang. The unprecedented spatial extent and intensity of the 2021 summer extreme heatwave event over the Western North American regions. Wea. Climate Extrem. **41**, 100576 (2023). https://doi.org/10.1016/j.wace.2023.100576.

[43] S. Bhattarai, L. Bokati, S. Sharma et al. Understanding spatiotemporal variation of heatwave projections across US cities. Sci. Rep. **15**, 10643 (2025). https://doi.org/10.1038/s41598-025-95097-5